

## Article

# Influence of Absorption Cross-Sections on Retrieving the Ozone Vertical Distribution at the Siberian Lidar Station

Sergey Dolgii <sup>1</sup>, Alexey A. Nevzorov <sup>2,\*</sup> , Alexey V. Nevzorov <sup>1</sup> , Yurii Gridnev <sup>3</sup>, Olga Kharchenko <sup>1</sup>  and Oleg A. Romanovskii <sup>2</sup> 

<sup>1</sup> Center of Laser Atmosphere Sensing, V.E. Zuev Institute of Atmospheric Optics SB RAS, 634055 Tomsk, Russia; dolgii@iao.ru (S.D.); nevzorov@iao.ru (A.V.N.); olya@iao.ru (O.K.)

<sup>2</sup> Laboratory for Remote Sensing of the Environment, V.E. Zuev Institute of Atmospheric Optics SB RAS, 634055 Tomsk, Russia; roa@iao.ru

<sup>3</sup> Laboratory of Optical Signals Propagation, V.E. Zuev Institute of Atmospheric Optics SB RAS, 634055 Tomsk, Russia; yuri@iao.ru

\* Correspondence: naa@iao.ru; Tel.: +7-382-249-0462

**Abstract:** The purpose of this paper is to study how the application of different sets of absorption cross-sections influence the ozone vertical distribution (OVD) in the upper layers of the troposphere—stratosphere in the altitude range ~ (5–45) km, using a differential absorption lidar (DIAL), operating at the sensing wavelengths 299/341 nm and 308/353 nm. We analyzed the results of lidar measurements of OVD obtained in 2021 using meteorological data from the IASI/MetOp satellite at the Siberian Lidar Station (SLS). The retrieval was performed using the data of four groups concerning the absorption cross-sections: Gorshelev et al., Malicet et al., SCIAMACHY, and GOME. To estimate how the absorption cross-sections influence the OVD retrieval from lidar measurements, we calculated the average deviations between the profiles retrieved using different sets both in a particular case on 2 January 2021 and throughout 2021. Our study showed that, out of the four absorption cross-section sets, the data of Gorshelev et al. should be used for long-term lidar monitoring of the ozone. These data show a more discrete dependence of the absorption cross-sections on the temperature values, which is more urgent for tropospheric and stratospheric ozone measurements.

**Keywords:** laser sensing; differential absorption; IASI; ozone and temperature-monitoring instruments



**Citation:** Dolgii, S.; Nevzorov, A.A.; Nevzorov, A.V.; Gridnev, Y.; Kharchenko, O.; Romanovskii, O.A. Influence of Absorption Cross-Sections on Retrieving the Ozone Vertical Distribution at the Siberian Lidar Station. *Atmosphere* **2022**, *13*, 293. <https://doi.org/10.3390/atmos13020293>

Academic Editor: Martin Dameris

Received: 9 December 2021

Accepted: 7 February 2022

Published: 9 February 2022

**Publisher's Note:** MDPI stays neutral with regard to jurisdictional claims in published maps and institutional affiliations.



**Copyright:** © 2022 by the authors. Licensee MDPI, Basel, Switzerland. This article is an open access article distributed under the terms and conditions of the Creative Commons Attribution (CC BY) license (<https://creativecommons.org/licenses/by/4.0/>).

## 1. Introduction

The problem of remote monitoring of minor gas constituents (MGCs) and aerosols in the atmosphere is urgent for constructing atmospheric models and for controlling Earth's climate change [1].

It is principally important that most of the radiatively active atmospheric constituents, i.e., clouds, aerosols, water vapor, and, especially, the ozone, are interrelated. For instance, the water vapor content of the atmosphere increases by evaporation during global warming. Depletion of the ozone layer leads to an increase in the incoming shortwave ultraviolet (UV) solar radiation. This results in an increase in the atmosphere of the strongest photooxidants OH and H<sub>2</sub>O<sub>2</sub> that stimulate the nucleation of aerosol, serving as condensation nuclei in the processes of cloud formation [2]. The increase of the temperature near the Earth's surface is known to be accompanied by temperature decrease in the troposphere, stratosphere, and mesosphere [3,4]. This should result in an increased probability of re-condensation clouds: cirrus clouds in the troposphere, nacreous clouds in the stratosphere, and noctilucent clouds in the mesosphere. From the viewpoint of the atmospheric radiation budget, the main climate-forming factors are cloud and aerosol fields, as well as greenhouse gases and, primarily, ozone and gas components of ozone cycles. Only stationary and mobile remote laser sensing or lidar sensing can provide information on ozone and aerosol distribution in the atmosphere at high speed and on large spatial scales [5–26]. It should be noted that

stationary lidar stations, similar to the Siberian Lidar Station (SLS), operate in different parts of the world: Tsukuba ( $36.05^{\circ}$  N,  $140.13^{\circ}$  E), Japan [5,6]; Observatoire de Haute Provence (OHP) ( $43.94^{\circ}$  N,  $5.71^{\circ}$  E), France [7,8]; Hefei ( $31.82^{\circ}$  N,  $117.22^{\circ}$  E), China [9,10]; Table Mountain Facility (TMF) ( $34.4^{\circ}$  N,  $117.7^{\circ}$  W), USA [11,12]; Goddard Space Flight Center (GSFC) ( $37.1^{\circ}$  N,  $76.39^{\circ}$  W), USA [13]; Vladivostok ( $43.3^{\circ}$  N,  $132^{\circ}$  E), Russia [14]; SLS or Tomsk ( $56.50^{\circ}$  N,  $85.00^{\circ}$  E), Russia [15,16]; Yangbajing Observatory ( $30^{\circ}5'$  N,  $90^{\circ}33'$  E), China [17]. There are modern mobile ozone lidars, located in trailers or on aircraft and united into a single research group. This USA group arranged a network of mobile lidars known as the Tropospheric Ozone Lidar Network (TOLNet) [18]: Goddard Space Flight Center TROPOspheric Ozone Differential Absorption Lidar (GSFC TROPOZ DIAL), Northeast of Washington, D.C. Greenbelt, Greenbelt, MD, USA [19]; Langley Mobile Ozone Lidar (LMOL), NASA Langley Research Center, Hampton, VA, USA [20]; Tunable Optical Profiler for Aerosol and Ozone (TOPAZ) system, NASA Langley Research Center, Hampton, VA, USA [21–23]; Autonomous Mobile Ozone Lidar Instrument for Tropospheric Experiments (AMOLITE) system, Air Quality Processes Research Section, Environment and Climate Change Canada, Toronto, Canada [24]; Langley Research Center airborne ozone lidar, NASA Langley Research Center, Hampton, VA, USA [25]. The SSRL (solid-state Raman laser) mobile lidar was created by Chinese scientists, Anhui Institute of Optics and Fine Mechanics of Chinese Academy of Sciences, Hefei [26]. An integral element of processing the results from laser monitoring is the application of the actual temperature-dependent absorption cross-sections of studied gas and most urgent meteorological data [27–31]. Therefore, the arising urgent need to present relevant recommendations on using the existing absorption cross-sections, applied to retrieve the ozone concentrations, and the problem of estimating their effect on the results obtained, started the activity of the Absorption Cross-Section of Ozone (ACSO) commission. The ACSO committee was established in 2008 as a joint initiative of the International Ozone Commission (IO3C), the World Meteorological Organization (WMO), and Integrated Global Atmospheric Chemistry Observations (IGACO) O<sub>3</sub>/UV subgroup on UV radiation for studying ozone absorption cross-sections. The ACSO proceeded to work within two time frames (2009–2011, 2013) [27]. Work [28], performed in the ACSO framework, compared the effects using three absorption cross-section datasets, i.e., Daumont, Brion and Malicet; Bass and Paur; Serdyuchenko and Gorshelev. These data were utilized to retrieve the ozone vertical distributions (OVD) from Ozone Monitoring Instrument (OMI) measurements in the wavelength range of 270–330 nm; the results were found to be biased by 5–10 DU. Comparison of results using Gorshelev/Bass and Paur datasets against ozonesondes showed considerable deviations up to 70%, in contrast to the application of Daumont and Brion/Malicet absorption cross-sections, which gave biases within 10%. In work [29], as a continuation of previous research, the data from the SCIAMACHY satellite spectrometer were added to analyze the temperature dependence of the existing absorption cross-sections. This work was furthered in studies of how absorption cross-section sets influence the ozone profiles from Global Ozone Monitoring Experiment (GOME) ultraviolet measurements in the wavelength ranges of 289–307 nm and 326–337 nm [30]. The result of the ACSO's work was presented in the final report [27].

In our previous work [31], we considered how temperature correction, and especially the absorption cross-sections from the works of Gorshelev et al. [32,33], influence the retrieval of ozone profiles in the upper troposphere–stratosphere when using a seasonal model of the temperature and the satellite-based temperature profiles. The retrieval results were subject to comparative analysis and showed that the application of temperature correction, using satellite-based temperature profiles, makes it possible to increase the information content of lidar sensing of the ozone in long-term monitoring at the wavelength pairs of 299/341 nm and 308/353 nm.

The purpose of this work is to study how different absorption cross-section sets influence the retrieved ozone profile in the stratosphere and in the upper troposphere–lower stratosphere (UTLS) in the altitude range of 5–45 km, using a differential absorption lidar (DIAL). In our work, the vertical distribution of ozone concentration was retrieved

by applying the data of four groups concerning absorption cross-sections: Gorshelev et al., Malicet et al. [34], SCIAMACHY [35], and GOME [36]. We analyzed the comparisons between the average profiles retrieved using the four groups of the absorption cross-sections. The result of the analysis are a justification for choosing urgent absorption cross-sections to be used for OVD retrieval in long-term lidar monitoring.

## 2. Lidar and Satellite Instruments

For the measurements of OVD at the wavelengths 299/341 and 308/353 nm in the altitude range of ~5–20 km and 15–45 km, at the SLS, a lidar complex is operated, implementing the work in the long-term monitoring mode in the UTLS and in the stratosphere [37]. The cycle of lidar measurements in the troposphere–stratosphere takes, on average, 1.5–2.5 h per day. In this period of time, two tropospheric and two stratospheric profiles of OVD are obtained at SLS. The main characteristics of the lidar complex were presented in detail in our previous work [16].

The Infrared Atmospheric Sounding Interferometer (IASI) is mounted onboard the meteorological satellite of the European Space Agency (MetOp) and works within the European Polar System Program. The interferometer measures such atmospheric constituents as CO<sub>2</sub>, CH<sub>4</sub>, N<sub>2</sub>O, CO, O<sub>3</sub>, and HNO<sub>3</sub>, as well as the air temperature and humidity profiles in the UTLS in the near-real-time mode. IASI provides high-radiometric quality spectra with a resolution of 0.5 cm<sup>−1</sup> in the range from 625 to 2760 cm<sup>−1</sup> [38]. IASI data are received with the help of a 2.4 XLB satellite information receiving station. We receive the temperature profiles from the satellite data receiving station with the spatial resolution of from ~150 m in the surface layer to several kilometers in the stratosphere and higher [39]. The obtained IASI data consists of 100 points in the high-altitude range 0.15–80 km.

The Microwave Limb Sounder (MLS) operates onboard the American scientific-research satellite Aura. The sounder measures atmospheric constituents such as BrO, CH<sub>3</sub>Cl, CO, ClO, HCl, HNO<sub>3</sub>, HO<sub>2</sub>, N<sub>2</sub>O, O<sub>3</sub>, etc., as well as the air temperature and humidity profiles in the stratosphere within the National Aeronautics and Space Administration (NASA) Earth Observing System Program. Our work uses the standard temperature data products obtained at 118 GHz in the stratosphere and 239 GHz in the troposphere [40,41]. MLS data are freely accessible on the NASA website [42]. The available MLS temperature profiles consist of 43 points with spatial resolution from about 1 km to several kilometers in the high-altitude range of 8–96 km.

Data from the SLS lidar complex are processed by introducing the meteorological data from MetOp or Aura. This is required for comparing the lidar and satellite OVDs, for studying the seasonal variations in the vertical distribution of ozone concentration, and for the long-term monitoring.

## 3. Measurement Technique

The lidar method of differential absorption and scattering envisages a comparison of signals returned from the atmosphere or lidar signals at two wavelengths, 299 or 308 nm (ozone absorption), and 341 or 353 nm (reference wavelengths). Analysis of the ratio of two lidar signals makes it possible to estimate the concentration of ozone in the atmosphere and its vertical distribution.

This method is actively used at all lidar stations around the world, where OVD is measured. It is based on the application of the equation from the works [43–45]:

$$n(H) = \frac{1}{2[k_{on}(H, T) - k_{off}(H, T)]} \times \frac{d}{dH} \left[ \ln \frac{N_{off}(H)}{N_{on}(H)} \right],$$

where  $n(H)$  is the concentration of ozone (10<sup>12</sup> molecules × cm<sup>−3</sup>) at the altitude  $H$ ,  $N_{on}(H)$  and  $N_{off}(H)$  are the return signals recorded (number of photons) at the wavelengths  $\lambda_{on}$  (on the absorption line) and  $\lambda_{off}$  (off the absorption line);  $k_{on}(H, T)$  and  $k_{off}(H, T)$  are the ozone absorption cross-sections (cm<sup>2</sup>/molecule) with the temperature dependence.

Real variations in the atmospheric temperature may cause substantial changes in a priori calculation of the ozone absorption coefficient, leading to systematic errors. Therefore, the OVD retrieval algorithm should be corrected for the temperature dependence using MetOp meteorological satellite data. The retrieval algorithm [34] incorporates the actual temperature dependence of the ozone absorption cross-section. In our work, we used the MetOp meteorological satellite data, and the absorption cross-sections from Gorshelev and Serdyuchenko, SCIAMACHY data, GOME data, and Malicet data for the wavelengths 299 and 341 nm, 308 and 353 nm. The absorption cross-section sets are distributed over wavelengths of 213–1100 nm and discrete values of the temperature. We sampled the absorption cross-sections according to the values close to the sensing wavelengths of the lidar complex. The sampling result is presented in Tables 1–4.

**Table 1.** The ozone absorption cross-sections (cm<sup>2</sup>/molecule) for two-wavelength pairs of ozone sensing from Gorshelev and Serdyuchenko [32,33].

Wavelength, nm	Temperature, K										
	193	203	213	223	233	243	253	263	273	283	293
Online											
299	$4.12 \times 10^{-19}$	$4.15 \times 10^{-19}$	$4.25 \times 10^{-19}$	$4.15 \times 10^{-19}$	$4.3 \times 10^{-19}$	$4.25 \times 10^{-19}$	$4.36 \times 10^{-19}$	$4.36 \times 10^{-19}$	$4.38 \times 10^{-19}$	$4.46 \times 10^{-19}$	$4.58 \times 10^{-19}$
308	$1.13 \times 10^{-19}$	$1.14 \times 10^{-19}$	$1.16 \times 10^{-19}$	$1.17 \times 10^{-19}$	$1.18 \times 10^{-19}$	$1.19 \times 10^{-19}$	$1.24 \times 10^{-19}$	$1.25 \times 10^{-19}$	$1.28 \times 10^{-19}$	$1.31 \times 10^{-19}$	$1.35 \times 10^{-19}$
Offline											
341	$5.62 \times 10^{-22}$	$5.94 \times 10^{-22}$	$6.1 \times 10^{-22}$	$6.95 \times 10^{-22}$	$7.05 \times 10^{-22}$	$7.59 \times 10^{-22}$	$8.15 \times 10^{-22}$	$8.9 \times 10^{-22}$	$9.9 \times 10^{-22}$	$1.08 \times 10^{-21}$	$1.15 \times 10^{-21}$
353	$4.95 \times 10^{-23}$	$6.4 \times 10^{-23}$	$7.25 \times 10^{-23}$	$8.88 \times 10^{-23}$	$9.57 \times 10^{-23}$	$1.1 \times 10^{-22}$	$1.27 \times 10^{-22}$	$1.45 \times 10^{-22}$	$1.67 \times 10^{-22}$	$2.02 \times 10^{-22}$	$2.38 \times 10^{-22}$

**Table 2.** Cross-sections (cm<sup>2</sup>/molecule) for two-wavelength pairs from Malicet data [34].

Wavelength, nm	Temperature, K				
	218	228	243	273	295
Online					
299	$4.1 \times 10^{-19}$	$4.1 \times 10^{-19}$	$4.25 \times 10^{-19}$	$4.3 \times 10^{-19}$	$4.6 \times 10^{-19}$
308	$1.2 \times 10^{-19}$	$1.2 \times 10^{-19}$	$1.2 \times 10^{-19}$	$1.26 \times 10^{-19}$	$1.36 \times 10^{-19}$
Offline					
341	$6 \times 10^{-22}$	$6 \times 10^{-22}$	$6 \times 10^{-22}$	$6 \times 10^{-22}$	$1.2 \times 10^{-21}$
353	$6.5 \times 10^{-23}$	$7.5 \times 10^{-23}$	$1 \times 10^{-22}$	$1.5 \times 10^{-22}$	$2.2 \times 10^{-22}$

**Table 3.** Cross-sections (cm<sup>2</sup>/molecule) for two-wavelength pairs from SCIAMACHY data [35].

Wavelength, nm	Temperature, K				
	203	223	243	273	293
Online					
299	$4.1 \times 10^{-19}$	$4.12 \times 10^{-19}$	$4.25 \times 10^{-19}$	$4.44 \times 10^{-19}$	$4.56 \times 10^{-19}$
308	$1.13 \times 10^{-19}$	$1.17 \times 10^{-19}$	$1.21 \times 10^{-19}$	$1.28 \times 10^{-19}$	$1.34 \times 10^{-19}$
Offline					
341	$5.59 \times 10^{-22}$	$6.74 \times 10^{-22}$	$7.61 \times 10^{-22}$	$9.67 \times 10^{-22}$	$1.14 \times 10^{-22}$
353	$6.06 \times 10^{-23}$	$8.58 \times 10^{-23}$	$1.15 \times 10^{-22}$	$1.73 \times 10^{-22}$	$2.42 \times 10^{-22}$

**Table 4.** Cross-sections (cm<sup>2</sup>/molecule) for two-wavelength pairs from GOME data [36].

Wavelength, nm	Temperature, K				
	202	221	241	273	293
<b>Online</b>					
299	$4.12 \times 10^{-19}$	$4.16 \times 10^{-19}$	$4.27 \times 10^{-19}$	$4.49 \times 10^{-19}$	$4.59 \times 10^{-19}$
308	$1.18 \times 10^{-19}$	$1.19 \times 10^{-19}$	$1.23 \times 10^{-19}$	$1.31 \times 10^{-19}$	$1.36 \times 10^{-19}$
<b>Offline</b>					
341	$5.74 \times 10^{-22}$	$6.25 \times 10^{-22}$	$7.16 \times 10^{-22}$	$9.49 \times 10^{-22}$	$1.13 \times 10^{-21}$
353	$5.72 \times 10^{-23}$	$6.93 \times 10^{-23}$	$9.91 \times 10^{-23}$	$1.86 \times 10^{-22}$	$2.41 \times 10^{-22}$

The absorption cross-section differential for different sets in a linear form is shown in Figure 1. From Figure 1, it can be seen that the absorption cross-sections are varied with the different steps of temperature points. Figure 1 shows the absorption cross-section differences with significant deviations for the wavelength pair 299–341 nm. However, for the wavelength pair 308–353 nm, the OACs from different data sets are close, especially for the SCIAMACHY and Gorshelev data. It is important to develop the works on refining the temperature dependence of absorption cross-sections, using temperature values not addressed before in other studies. Particularly, as shown in Figure 1a, the oscillations in the difference between absorption cross-sections strongly vary from one point to another, according to the data of Gorshelev and Serdyuchenko. This work will significantly improve the reliability of lidar measurements.

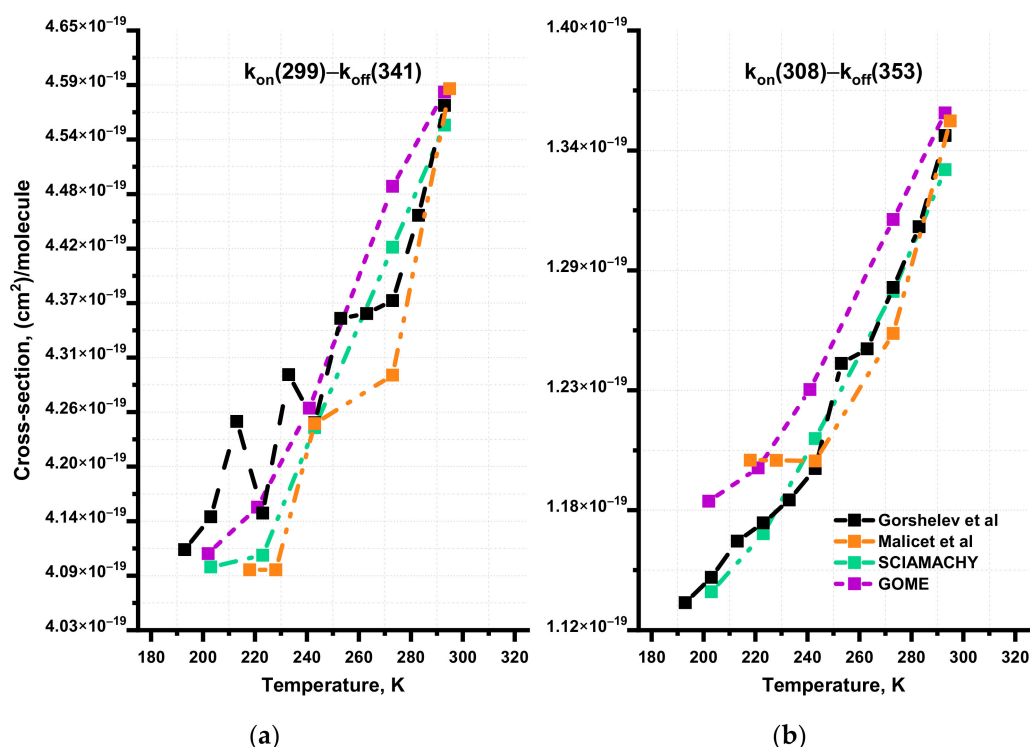


**Figure 1.** The differential ozone absorption cross-sections (i.e.,  $k_{on}-k_{off}$ ), for (a) 299/341 nm and (b) 308/353 nm derived from four different datasets: SCIAMACHY, GOME, Malicet, and Gorshelev.

Data from the work of Gorshelev and Serdyuchenko are among the best absorption cross-section sets to date. They were the last experimenters known to measure the absorption cross-sections and take into consideration all the previous results. They used two types of spectrometers (Echelle and Fourier transform), which made it possible to

obtain new broadband absorption cross-sections of ozone, covering the wavelength range from UV to NIR (213–1100 nm). In their work, they achieved the absorption cross-section measurements at the record low temperature of 193 K and carried out a step in the temperature values of 10 K for the absorption cross-section measurements, as compared to the 20 K step in the GOME and SCIAMACHY, Malicet data. As a result, the number of discrete temperature-dependent absorption cross-sections according to the Gorshelev and Serdyuchenko data is about two times greater than can be obtained using GOME and SCIAMACHY, Malicet values. To solve the inverse problem of retrieving the ozone concentration from the data of lidar sensing, we preferred to choose the results from Gorshelev and Serdyuchenko because the error of all absorption cross-section sets is within  $\sim 3\%$ .

#### 4. Results and Discussion

During 2021, we carried out more than 100 measurements in the stratosphere and in the UTLS. Using the method of differential absorption and scattering, with the incorporation of the actual temperature measurements from MetOp and different sets of absorption cross-sections into the retrieval algorithm, we calculated the average ozone profiles for the stratosphere and UTLS. In this work, we used those results for analysis to clarify precisely how different absorption cross-sections will influence the long-term measurements of the vertical distribution of ozone concentration. Analysis of the temperature correction in applying model- and satellite-based vertical distributions of the temperature was carried out in our previous work [31].

For a particular case of measurements on 2 January 2021, as an example, Figure 2 shows how the sets of the absorption cross-sections were used to influence the deviation of ozone profiles obtained. We have reduced the altitude and ozone concentration ranges to show more clearly the difference between the profiles. At the stratospheric heights near the ozone maximum, significant profile deviations are present. It can be seen that the retrieved ozone profiles using Gorshelev and SCIAMACHY absorption cross-sections are very close. The difference between the SCIAMACHY and Malicet ozone profiles at 18.5 km altitude reaches  $0.27 \times 10^{12}$  molecules  $\times$  cm $^{-3}$  or  $\sim 4.5$ . The obtained tropospheric profiles have close values over the entire altitude interval. The difference between the Gorshelev and Malicet ozone profiles at 13 km altitude reaches  $0.11 \times 10^{12}$  molecules  $\times$  cm $^{-3}$ , or  $\sim 4\%$ .

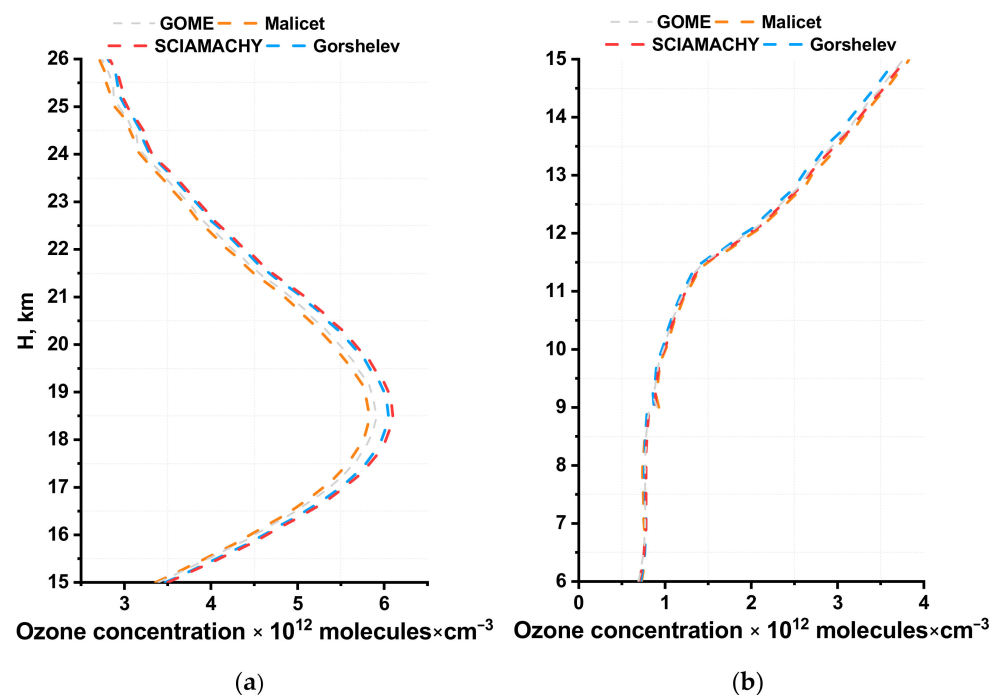
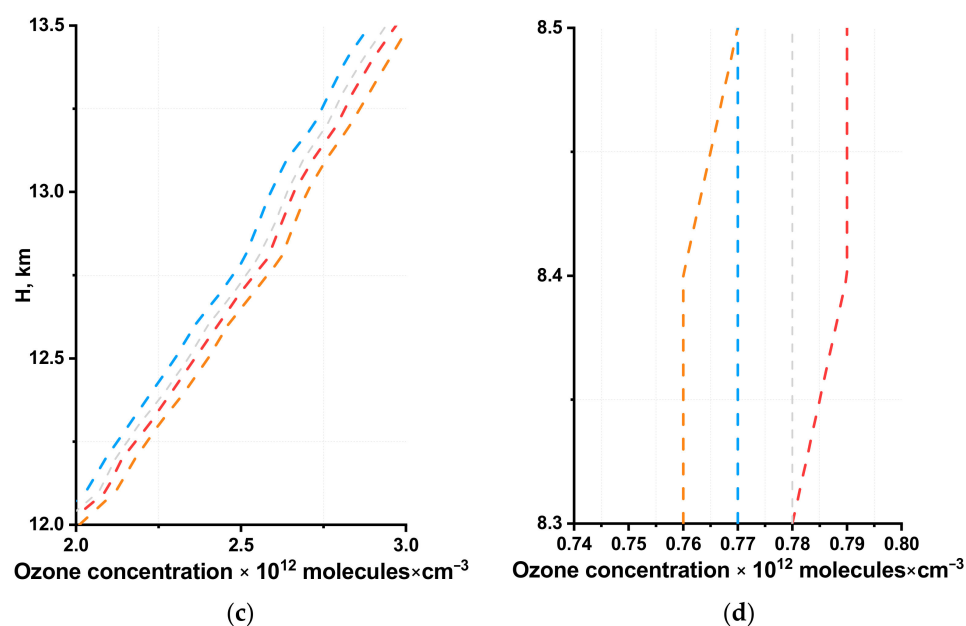


Figure 2. Cont.



**Figure 2.** Ozone vertical distributions, retrieved using different absorption cross-sections and MetOp meteorological data: (a) stratospheric ozone profiles, (b) tropospheric ozone profile, (c) zoomed-in UTLS, and (d) tropospheric ozone profiles.

We note that the deviations presented in Figure 2 are very close. To demonstrate the most visible differences in the stratosphere, we facilitated a transect at 18.5 km. The transect showed that the retrieved profiles have the following values:  $5.83 \times 10^{12}$  molecules  $\times$  cm $^{-3}$  for Malicet,  $6.05 \times 10^{12}$  molecules  $\times$  cm $^{-3}$  for Gorshelev,  $6.1 \times 10^{12}$  molecules  $\times$  cm $^{-3}$  for SCIAMACHY, and  $5.91 \times 10^{12}$  molecules  $\times$  cm $^{-3}$  for GOME. At the same time, when considered on an enlarged scale as in Figure 2c, the ozone vertical profiles, obtained applying different sets of absorption cross-sections, do not intersect with each other and are within the retrieval error of ~6–14% for the altitudes of 5–20 km and within 5% for the stratospheric altitudes at the spatial resolution of 100 m.

We will consider the statistical characteristics of how the absorption cross-section sets influence the OVD behavior in the framework of 2021 lidar measurements. The series of ozone profiles were retrieved using different absorption cross-section sets from the same lidar signals. Calculating the average over each series gave us the difference between the profiles: between Gorshelev and SCIAMACHY, Gorshelev and Malicet, Gorshelev and GOME, SCIAMACHY and GOME, SCIAMACHY and Malicet, and GOME and Malicet. Figure 3 presents the differences between the average profiles graphically.

We covered the altitude interval within 15–40 km to better represent the data obtained from the stratospheric measurements. From Figure 3, it can be seen that the closeness of OVDs, retrieved using Gorshelev and SCIAMACHY absorption cross-sections is statistically confirmed. We note that the largest deviations between the differences are recorded at the altitudes of the stratospheric maximum, ~20–22 km. From Figure 3, it can be seen that within ~20–22 km, SCIAMACHY/Malicet has a maximum of  $0.25 \times 10^{12}$  molecules  $\times$  cm $^{-3}$  at the altitude of 20.7 km, GOME/Malicet has a maximum of  $0.08 \times 10^{12}$  molecules  $\times$  cm $^{-3}$  at the altitude of 20.7 km, SCIAMACHY/GOME has a maximum of  $0.17 \times 10^{12}$  molecules  $\times$  cm $^{-3}$  at the altitude of 20.7 km, Gorshelev/GOME has a maximum of  $0.13 \times 10^{12}$  molecules  $\times$  cm $^{-3}$  at the altitude of 20.7 km, and Gorshelev/SCIAMACHY has a maximum vertical distribution of  $-0.05 \times 10^{12}$  molecules  $\times$  cm $^{-3}$  at the altitude of 21.2 km. This pattern is characteristic of the Gorshelev/Malicet difference between the average profiles, in which case it is  $0.21 \times 10^{12}$  molecules  $\times$  cm $^{-3}$  at the altitude of 21.1 km.

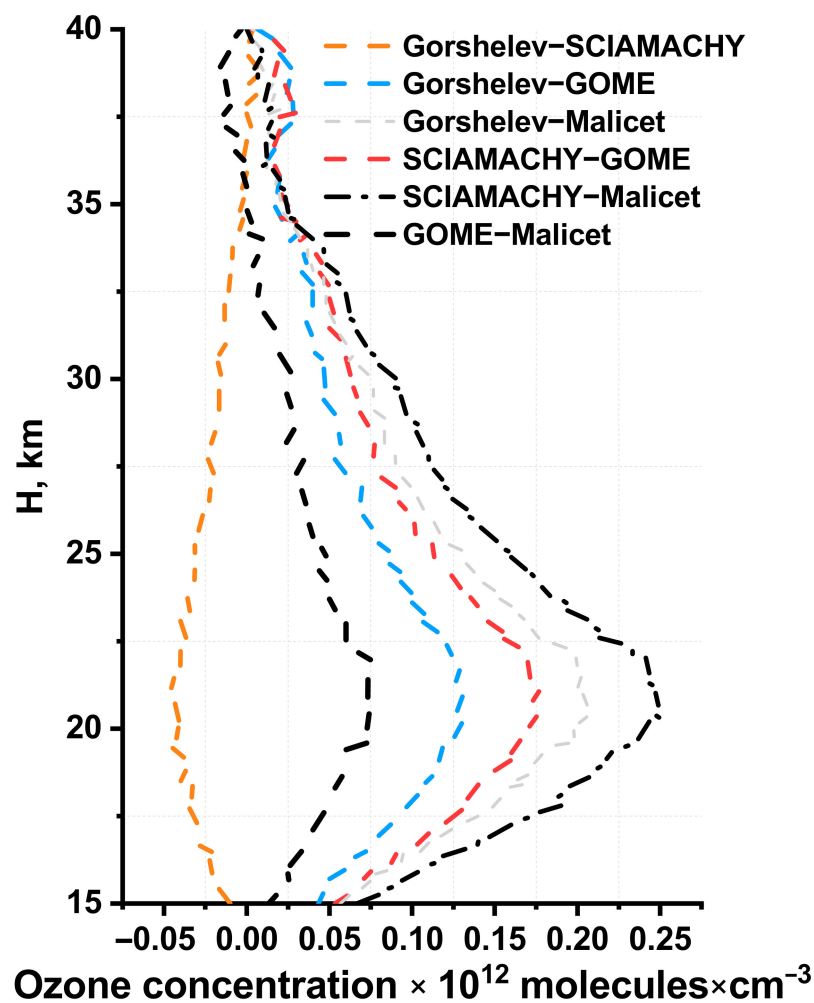


**Figure 3.** Ozone vertical distributions, retrieved using different absorption cross-sections and MetOp meteorological data: stratospheric ozone profile differences.

In a similar way, we calculated the differences for the average profiles in the UTLS. These results are presented graphically in Figure 4.

Figure 4 statistically confirms that the biggest average profile for all altitudes was obtained using Maliget absorption cross-sections. Next are the average profile with SCIAMACHY absorption cross-sections and the profiles from GOME and Gorshchelev. For a particular case, this is also confirmed in Figure 2. We note that a break at altitudes of 12–13 km near the tropopause is discernible for the difference between the average profiles of Gorshchelev/Maliget, SCIAMACHY/Maliget, and GOME/Maliget. From Figure 4, it can be seen that, within the altitude range of 6.5–7 km, there is a zero difference, i.e., there is no difference between the average profiles at these altitudes. However, outside this altitude range, there are minimal values, close to zero. The maximal deviations ( $-0.13 \times 10^{12}$  molecules  $\times$  cm $^{-3}$ ) are found between Gorshchelev and Maliget at the altitude of 13.1 km; and the minimal differences ( $-0.03 \times 10^{12}$  molecules  $\times$  cm $^{-3}$ ) between them are at the altitude of 7.7 km. The minimal deviations between Gorshchelev and GOME are  $-0.003 \times 10^{12}$  molecules  $\times$  cm $^{-3}$  at the altitude of 7.7 km; and the maximal deviations reach  $-0.11 \times 10^{12}$  molecules  $\times$  cm $^{-3}$  at the altitude of 19.2 km. In a similar way, there are maximal deviations between SCIAMACHY and Maliget of  $0.15 \times 10^{12}$  molecules  $\times$  cm $^{-3}$  at the altitude of 19.6 km and minimal deviations of  $-0.01 \times 10^{12}$  molecules  $\times$  cm $^{-3}$  at the altitude of 7.3 km. The Gorshchelev and SCIAMACHY have maximal deviations of  $-0.15 \times 10^{12}$  molecules  $\times$  cm $^{-3}$  at the altitude of 19.4 km, and the minimal differences ( $-0.003 \times 10^{12}$  molecules  $\times$  cm $^{-3}$ ) between them are at the altitude of 7.1 km. These devia-

tions are very significant for tropospheric altitudes. The meteorological data and absorption cross-sections applied for profile retrieval are very important for such altitudes. Generally, we use meteorological data from the MetOp satellite, and absorption cross-sections from Gorshelev and Serdyuchenko. They are most relevant to our studies and influence appreciably the results in studies of the ozonosphere dynamics.

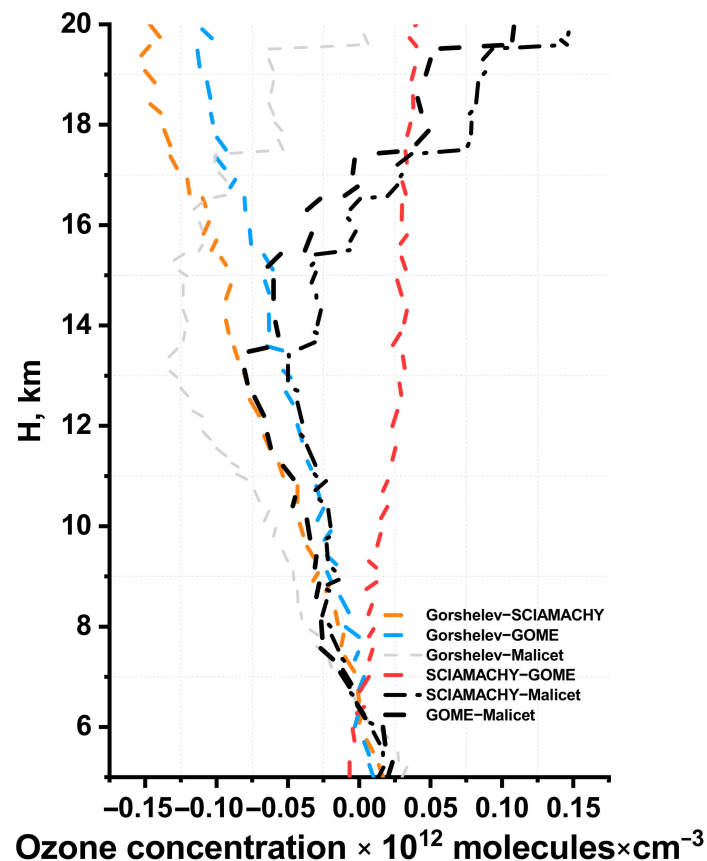


**Figure 4.** Ozone vertical distributions, retrieved using different absorption cross-sections and MetOp meteorological data: tropospheric ozone profile differences.

## 5. Conclusions

In this paper, we present the deviations of ozone profiles, averaged over all measurements obtained over 2021. This is sufficient to estimate the general pattern, where there is the effect from applying absorption cross-section sets at the altitudes of the stratosphere and troposphere. The analysis of comparisons of ozone profiles for different absorption cross-section sets and their average deviations showed that for lidar monitoring, it is acceptable to use the data from the works of Gorshelev and Serdyuchenko, especially at tropospheric altitudes. The effect of using different data is more pronounced at tropospheric altitudes around tropopause at the wavelengths 299/341 nm, where the used absorption cross-section sets strongly vary from one point to another. The temperature dependence of the absorption cross-sections will influence the behavior of ozone profiles in the troposphere and stratosphere more heavily after the addition of earlier unexplored temperature quantities, thus substantially increasing the reliability of the OVD retrievals. In the OVD retrievals, one should not use the data of Maliget because they strongly overestimate the ozone concentrations in the troposphere and underestimate them in the stratosphere. Of the four absorption cross-section sets, we recommend using the Gorshelev data because they give more detailed information on the absorption cross-sections over discrete values of the temperature, which is very important for lidar sensing of the troposphere where the factor of temperature variations is great. In the stratosphere, the SCIAMACHY data provides

slightly more overestimated ozone concentrations than Gorshelev. However, considering that when ozone anomalies occur, it is important to take into account more pronounced temperature variations, Gorshelev data should be considered as an ultimate choice of the absorption cross-sections for retrievals at stratospheric altitudes.

**Author Contributions:** Conceptualization, S.D., A.V.N., A.A.N., O.A.R. and O.K.; methodology, A.V.N. and A.A.N.; validation, A.A.N. and A.V.N.; formal analysis, A.A.N.; resources, A.V.N., S.D., Y.G. and A.A.N.; data curation, A.V.N., S.D., Y.G. and A.A.N.; writing—original draft preparation, A.A.N.; writing—review and editing, A.A.N.; visualization, A.A.N.; supervision, A.A.N.; project administration, O.A.R. and A.A.N. All authors have read and agreed to the published version of the manuscript.

**Funding:** This work was funded by the Russian Science Foundation No. 21-79-10051.

**Acknowledgments:** The authors wish to thank I.V. Ptashnik from the V.E. Zuev Institute of Atmospheric Optics of the Siberian Branch of the Russian Academy of Science.

**Conflicts of Interest:** The authors declare no conflict of interest.

## References

1. Weitkamp, C. *Lidar: Range Resolved Optical Remote Sensing of the Atmosphere*; Springer: Berlin/Heidelberg, Germany, 2005; pp. 1–18.
2. Monod, A.; Liu, Y. Aerosol formation and heterogeneous chemistry in the atmosphere. *EPJ Web Conf.* **2011**, *18*, 04002. [[CrossRef](#)]
3. Perevedentsev, Y.P.; Shantalinskii, K.M.; Sherstyukov, B.G.; Guryanov, V.V. Current Climatic Changes in the Troposphere, Stratosphere, and Mesosphere, and Inter-Layer Interactions. *IOP Conf. Ser. Earth Environ. Sci.* **2019**, *386*, 012003. [[CrossRef](#)]
4. Goessling, H.F.; Bathiany, S. Why CO<sub>2</sub> cools the middle atmosphere—A consolidating model perspective. *Earth Syst. Dynam.* **2016**, *7*, 697–715. [[CrossRef](#)]
5. Park, C.B.; Nakane, H.; Sugimoto, N.; Matsui, I.; Sasano, Y.; Fujinuma, Y.; Ikeuchi, I.; Kurokawa, J.-I.; Furuhashi, N. Algorithm improvement and validation of National Institute for Environmental Studies ozone differential absorption lidar at the Tsukuba Network for Detection of Stratospheric Change complementary station. *Appl. Opt.* **2006**, *45*, 3561–3576. [[CrossRef](#)] [[PubMed](#)]
6. Nakazato, M.; Nagai, T.; Sakai, T.; Hirose, Y. Tropospheric ozone differential-absorption lidar using stimulated Raman scattering in carbon dioxide. *Appl. Opt.* **2007**, *46*, 2269–2279. [[CrossRef](#)] [[PubMed](#)]
7. Godin, S.; Bergeret, V.; Bekki, S.; David, C.; Mégie, G. Study of the interannual ozone loss and the permeability of the Antarctic Polar Vortex from long-term aerosol and ozone lidar measurements in Dumont d’Urville (66.4°, 140° S). *J. Geophys. Res.* **2001**, *106*, 1311–1330. [[CrossRef](#)]
8. Gaudel, A.; Ancellet, G.; Godin-Beekmann, S. Analysis of 20 years of tropospheric ozone vertical profiles by lidar and ECC at Observatoire de Haute Provence (OHP) at 44° N, 6.7° E. *Atmos. Environ.* **2015**, *113*, 78–89. [[CrossRef](#)]
9. Hu, S.; Hu, H.; Wu, Y.; Zhou, J.; Qi, F.; Yue, G. Atmospheric ozone measured by differential absorption lidar over Hefei. *Proc. SPIE* **2003**, 4893. [[CrossRef](#)]
10. Liu, X.; Zhang, Y.; Hu, H.; Tan, K.; Tao, Z.; Shao, S.; Cao, K.; Fang, X.; Yu, S. Mobile lidar for measurements of SO<sub>2</sub> and O<sub>3</sub> in the low troposphere. *Proc. SPIE* **2005**, 5832. [[CrossRef](#)]
11. McDermid, I.S.; Godin, S.M.; Lindquist, L.O. Ground-based laser DIAL system for long-term measurements of stratospheric ozone. *Appl. Opt.* **1990**, *29*, 3603–3612. [[CrossRef](#)]
12. McDermid, I.S.; Beyerle, G.; Haner, D.A.; Leblanc, T. Redesign and improved performance of the tropospheric ozone lidar at the Jet Propulsion Laboratory Table Mountain Facility. *Appl. Opt.* **2002**, *41*, 7550–7555. [[CrossRef](#)] [[PubMed](#)]
13. Steinbrecht, W.; McGee, T.J.; Twigg, L.W.; Claude, H.; Schönnenborn, F.; Sumnicht, G.K.; Silbert, D. Intercomparison of stratospheric ozone and temperature profiles during the October 2005 Hohenpeißenberg Ozone Profiling Experiment (HOPE). *Atmos. Meas. Tech.* **2009**, *2*, 125–145. [[CrossRef](#)]
14. Pavlov, A.N.; Stolyarchuk, S.Y.; Shmirko, K.A.; Bukin, O.A. Lidar Measurements of Variability of the Vertical Ozone Distribution Caused by the Stratosphere–Troposphere Exchange in the Far East Region. *Atmos. Ocean. Opt.* **2013**, *26*, 126–134. [[CrossRef](#)]
15. Burlakov, V.D.; Dolgii, S.I.; Nevzorov, A.V. Modification of the measuring complex at the Siberian Lidar Station. *Atmos. Ocean. Opt.* **2004**, *17*, 756–762.
16. Dolgii, S.I.; Nevzorov, A.A.; Nevzorov, A.V.; Romanovskii, O.A.; Makeev, A.P.; Kharchenko, O.V. Lidar Complex for Measurement of Vertical Ozone Distribution in the Upper Troposphere–Stratosphere. *Atmos. Ocean. Opt.* **2018**, *31*, 702–708. [[CrossRef](#)]
17. Fang, X.; Li, T.; Ban, C.; Wu, Z.; Li, J.; Li, F.; Cen, Y.; Tian, B. A mobile differential absorption lidar for simultaneous observations of tropospheric and stratospheric ozone over Tibet. *Opt. Express* **2019**, *27*, 4126–4139. [[CrossRef](#)]
18. Leblanc, T.; Brewer, M.A.; Wang, P.S.; Granados-Muñoz, M.J.; Strawbridge, K.B.; Travis, M.; Firanski, B.; Sullivan, J.T.; McGee, T.J.; Sumnicht, G.K.; et al. Validation of the TOLNet lidars: The Southern California Ozone Observation Project (SCOOP). *Atmos. Meas. Tech.* **2018**, *11*, 6137–6162. [[CrossRef](#)]

19. Sullivan, J.T.; McGee, T.J.; Sumnicht, G.K.; Twigg, L.W.; Hoff, R.M. A mobile differential absorption lidar to measure sub-hourly fluctuation of tropospheric ozone profiles in the Baltimore–Washington, D.C. region. *Atmos. Meas. Tech.* **2014**, *7*, 3529–3548. [[CrossRef](#)]
20. De Young, R.; Carrion, W.; Ganoë, R.; Pliutau, D.; Gronoff, G.; Berkoff, T.; Kuang, S. Langley mobile ozone lidar: Ozone and aerosol atmospheric profiling for air quality research. *Appl. Opt.* **2017**, *56*, 721–730. [[CrossRef](#)]
21. Alvarez, R.J.; Senff, C.J.; Langford, A.O.; Weickmann, A.M.; Law, D.C.; Machol, J.L.; Merritt, D.A.; Marchbanks, R.D.; Sandberg, S.P.; Brewer, W.A.; et al. Development and Application of a Compact, Tunable, Solid-State Airborne Ozone Lidar System for Boundary Layer Profiling. *J. Atmos. Ocean. Technol.* **2011**, *28*, 1258–1272. [[CrossRef](#)]
22. Wang, L.; Newchurch, M.; Alvarez, R.; Berkoff, T.; Brown, S.; Carrion, W.; De Young, R.; Johnson, B.; Ganoë, R.; Gronoff, G.; et al. Quantifying TOLNet ozone lidar accuracy during the 2014 DISCOVER-AQ and FRAPPÉ campaigns. *Atmos. Meas. Tech.* **2017**, *10*, 3865–3876. [[CrossRef](#)] [[PubMed](#)]
23. Alvarez, R.J.; Senff, C.J.; Weickmann, A.M.; Sandberg, S.P.; Langford, A.O.; Marchbanks, R.D.; Brewer, W.A.; Hardesty, R.M. Reconfiguration of the NOAA TOPAZ Lidar for Ground-based Measurement of Ozone and Aerosol Backscatter. In Proceedings of the 26th International Laser Radar Conference, Porto Heli, Greece, 25–29 June 2012; pp. 249–252.
24. Strawbridge, K.B.; Travis, M.S.; Firanski, B.J.; Brook, J.R.; Staebler, R.; Leblanc, T. A fully autonomous ozone, aerosol and nighttime water vapor lidar: A synergistic approach to profiling the atmosphere in the Canadian oil sands region. *Atmos. Meas. Tech.* **2018**, *11*, 6735–6759. [[CrossRef](#)]
25. Browell, E.V.; Ismail, S.; Grant, W.B. Differential absorption lidar (DIAL) measurements from air and space. *Appl. Phys. B* **1998**, *67*, 399–410. [[CrossRef](#)]
26. Liu, P.; Zhang, T.; Sun, X.; Fan, G.; Xiang, Y.; Fu, Y.; Dong, Y. Compact and movable ozone differential absorption lidar system based on an all-solid-state, tuning-free laser source. *Opt. Express.* **2020**, *28*, 13786–13800. [[CrossRef](#)] [[PubMed](#)]
27. Orphal, J.; Staehelin, J.; Tamminen, J.; Braathen, G.; De Backer, M.-R.; Bais, A.; Balis, D.; Barbe, A.; Bhartia, P.K.; Birk, M.; et al. Absorption cross-sections of ozone in the ultraviolet and visible spectral regions: Status report 2015. *J. Mol. Spectrosc.* **2016**, *327*, 105–121. [[CrossRef](#)]
28. Liu, C.; Liu, X.; Chance, K. The impact of using different ozone cross sections on ozone profile retrievals from OMI UV measurements. *J. Quant. Spectrosc. Radiat. Transf.* **2013**, *130*, 365–372. [[CrossRef](#)]
29. Wang, H.; Chai, S.; Tang, X.; Zhou, B.; Bian, J.; Zheng, X.D.; Vomel, H.; Yu, K.; Wang, W. Application of temperature dependent ozone absorption cross-sections in total ozone retrieval at Kunming and Hohenpeissenberg stations. *Atmos. Environ.* **2019**, *215*, 116890. [[CrossRef](#)]
30. Liu, X.; Chance, K.; Sioris, C.E.; Kurosu, T.P. Impact of using different ozone cross sections on ozone profile retrievals from Global Ozone Monitoring Experiment (GOME) ultraviolet measurements. *Atmos. Chem. Phys.* **2007**, *7*, 3571–3578. [[CrossRef](#)]
31. Dolgii, S.I.; Nevzorov, A.A.; Nevzorov, A.V.; Gridnev, Y.; Kharchenko, O.V. Temperature Correction of the Vertical Ozone Distribution Retrieval at the Siberian Lidar Station Using the MetOp and Aura Data. *Atmosphere* **2020**, *11*, 1139. [[CrossRef](#)]
32. Gorshelev, V.; Serdyuchenko, A.; Weber, M.; Chehade, W.; Burrows, J.P. High spectral resolution ozone absorption cross-sections—Part 1: Measurements, data analysis and comparison with previous measurements around 293 K. *Atmos. Meas. Tech.* **2014**, *7*, 609–624. [[CrossRef](#)]
33. Serdyuchenko, A.; Gorshelev, V.; Weber, M.; Chehade, W.; Burrows, J.P. High spectral resolution ozone absorption cross-sections—Part 2: Temperature dependence. *Atmos. Meas. Tech.* **2014**, *7*, 625–636. [[CrossRef](#)]
34. Malicet, J.; Daumont, D.; Charbonnier, J.; Parisse, A.; Chakir, A.; Brion, J. Ozone UV spectroscopy 2. Absorption cross-sections and temperature-dependence. *J. Atmos. Chem.* **1995**, *21*, 263–273. [[CrossRef](#)]
35. Molecular Spectroscopy and Chemical Kinetics Group Studies at the IUP, University of Bremen. Temperature Dependent Absorption Cross Sections Measured with the SCIAMACHY Satellite Spectrometer. Version 4.0 for Ozone. Available online: <https://www.iup.uni-bremen.de/gruppen/molspec/databases/sciamachydata/index.html> (accessed on 9 December 2021).
36. Molecular Spectroscopy and Chemical Kinetics Group Studies at the IUP, University of Bremen. Temperature-Dependent Absorption Cross-Sections of O<sub>3</sub> in the 231–794 nm Range Recorded with GOME FM. O<sub>3</sub> Data. Available online: <https://www.iup.uni-bremen.de/gruppen/molspec/databases/gomefmdata/index.html> (accessed on 9 December 2021).
37. Burlakov, V.D.; Dolgii, S.I.; Nevzorov, A.A.; Nevzorov, A.V.; Gridnev, Y.; Kharchenko, O.V. Measurements of Ozone Vertical Profiles in the Upper Troposphere–Stratosphere over Western Siberia by DIAL, MLS, and IASI. *Atmosphere* **2020**, *11*, 196. [[CrossRef](#)]
38. August, T.; Klaes, D.; Schlüssel, P.; Hultberg, T.; Crapeau, M.; Arriaga, A.; O’Carroll, A.; Coppens, D.; Munro, R.; Calbet, X. IASI on Metop-A: Operational Level 2 retrievals after five years in orbit. *J. Quant. Spectrosc. Radiat. Transf.* **2012**, *113*, 1340–1371. [[CrossRef](#)]
39. Matvienko, G.G.; Belan, B.D.; Panchenko, M.V.; Romanovskii, O.A.; Sakerin, S.M.; Kabanov, D.M.; Turchinovich, S.A.; Turchinovich, Y.S.; Eremina, T.A.; Kozlov, V.S.; et al. Complex experiment on studying the microphysical, chemical, and optical properties of aerosol particles and estimating the contribution of atmospheric aerosol-to-earth radiation budget. *Atmos. Meas. Tech.* **2015**, *8*, 4507–4520. [[CrossRef](#)]
40. Waters, J.W.; Froidevaux, L.; Harwood, R.S.; Jarnot, R.F.; Pickett, H.M.; Read, W.G.; Siegel, P.H.; Cofield, R.E.; Filipiak, M.J.; Flower, D.A.; et al. The Earth Observing System Microwave Limb Sounder (EOS MLS) on the Aura Satellite. *IEEE TGRS Trans. Geosci. Remote Sens.* **2006**, *44*, 1075–1092. [[CrossRef](#)]

41. NASA (National Aeronautics and Space Administration). Microwave Limb Sounder. The MLS Temperature Product. Available online: [https://mls.jpl.nasa.gov/products/temp\\_product.php](https://mls.jpl.nasa.gov/products/temp_product.php) (accessed on 9 December 2021).
42. NASA (National Aeronautics and Space Administration). MLS Temperature Data. Available online: <https://avdc.gsfc.nasa.gov/pub/data/satellite/Aura/MLS/> (accessed on 9 December 2021).
43. Measures, R.M. *Laser Remote Sensing: Fundamentals and Applications*; Reprint 1984 de Krieger Publishing Company; Krieger Publishing Company: Malabar, FL, USA, 1992; pp. 237–280.
44. Burlakov, V.D.; Dolgii, S.I.; Nevzorov, A.A.; Nevzorov, A.V.; Romanovskii, O.A. Algorithm for Retrieval of Vertical Distribution of Ozone from DIAL Laser Remote Measurements. *Opt. Mem. Neural Netw. Inf. Opt.* **2015**, *24*, 295–302. [[CrossRef](#)]
45. Dolgii, S.I.; Nevzorov, A.A.; Nevzorov, A.V.; Romanovskii, O.A.; Kharchenko, O.V. Intercomparison of Ozone Vertical Profile Measurements by Differential Absorption Lidar and IASI/MetOp Satellite in the Upper Troposphere-Lower Stratosphere. *Remote Sens.* **2017**, *9*, 447. [[CrossRef](#)]